Authors

Daniel W McKay[1], Yue Qu[1], Heather E McFarlane[2,3], Apriadi Situmorang[1], Matthew Gilliham[1] and Stefanie Wege[1,*]

Affiliations

[1]ARC Centre of Excellence in Plant Energy Biology, PRC, School of Agriculture, Food and Wine, Waite Research Institute, University of Adelaide, Waite Campus, Glen Osmond 5064, South Australia, Australia

[2]School of Biosciences, University of Melbourne, Melbourne, VIC 3010, Australia

[3]Present address: Department of Cell and Systems Biology, University of Toronto, Toronto, ON, M5S 3G5, Canada

*Correspondence: stefanie.wege@adelaide.edu.au

Title

Endomembrane Cation Chloride Cotransporters (CCC1s) modulate endo- and exocytosis

Short title

CCC1 modulates endomembrane trafficking

One sentence summary

Cation Chloride Cotransporters function in the TGN/EE and modulate endo- and exocystosis, impacting root cell identity, root hair elongation, osmoregulation and cell wall formation.

Material distribution footnote

The author responsible for distribution of materials integral to the findings presented in this article in accordance with the policy described in the Instructions for Authors (www.plantcell.org) is: Stefanie Wege (stefanie.wege@adelaide.edu.au)

Abstract

The secretary and endocytic pathways intersect at the *trans*-Golgi network/Early Endosome (TGN/EE). TGN/EE function depends on a careful balance of ions within this compartment, and the electrochemical potential across its membrane. The identity of the proton pump required for acidification and the transporters that catalyse cation and anion import into endosome compartments are known. However, the protein needed to complete the transport circuit, and that mediates cation and anion efflux from the TGN/EE has not been identified. Here, we characterize Cation Chloride Cotransporters (CCC1s) from Arabidopsis and rice. We find that the AtCCC1 is localized to the TGN/EE, where it modulates important TGN functions such as endocytosis, exocytosis, and cell wall synthesis/secretion. Loss of CCC1 results in severe, widespread phenotypes in both rice and Arabidopsis, including plant growth and developmental perturbations, defects in root hair elongation and altered osmoregulation, consistent with CCC performing a core cellular function. Complementation of the root hair elongation phenotype of *Atccc1* with root hair specific expression of GFP-AtCCC1 demonstrates CCC1 functions within the TGN/EE. Collectively, our results imply that CCC1 is a strong candidate for the missing component of the TGN/EE ion transportcircuit.

Introduction

Cellular function is dependent upon ion transport across endomembranes (Sze and Chanroj, 2018). Organisms lacking key endomembrane ion transporters often exhibiting severe phenotypic defects (Maresova and Sychrova, 2005; Colmenero-Flores et al., 2007; Jentsch and Pusch, 2018). Despite this, the roles of the transport proteins resident within compartments such as the Endoplasmic Reticulum (ER), Golgi, *trans*-Golgi-network/Early-Endosome (TGN/EE) or Pre-Vacuolar-Compartment (PVC) are, in general, poorly

characterised compared to proteins resident within the plasma membrane (PM) or tonoplast. Among the few examples of characterised proteins are the TGN/EE and ER localised Arabidopsis sodium/potassium proton exchangers NHX5 and NHX6 and the potassium proton exchangers KEA4, KEA5 and KEA6. These proteins were shown to fulfil important roles in protein sorting to the vacuole, sorting of the auxin transporter PIN5, and potassium homeostasis; and the respective double or triple knockouts exhibit severely stunted growth (Bassil et al., 2011; Fan et al., 2018; Zhu et al., 2018; Wang et al., 2019). The cation proton exchanger CHX20 localises to the endomembrane system and was shown to be important for osmoregulation of stomatal guard cells (Sze et al., 2004; Padmanaban et al., 2007) and the ER localised soybean CHX protein, GmSALT3, was shown to be important for salinity tolerance (Guan et al., 2014; Liu et al., 2016). Lastly, the TGN/EE localised chloride proton antiporter CLC-d was shown to be important for pathogen resistance (Guo et al., 2014). Such wide-ranging and pleiotropic phenotypes are typical of plants with defects in Golgi/TGN function (Dettmer et al., 2006; Richter et al., 2007; Teh and Moore, 2007; Gendre et al., 2011; Gendre et al., 2013; Ravikumar et al., 2018); however, the reasons that such a diverse set of phenotypes are caused by the loss of these endomembrane transporters is currently not well understood.

Here we investigate the cellular function of plant CCC1 proteins, which are large membrane proteins, typically around 1000 amino acid length; they are membrane-integrated, function as dimers and mediate electroneutral ion transport (Henderson et al., 2018; Liu et al., 2019). Plants usually contain 1-3 *CCC1* homologues per genome, and angiosperm plants do not contain *CCC2* homologues (Henderson et al., 2018). Rice harbours two, *OsCCC1.1* and *OsCCC1.2*, and Arabidopsis one, *AtCCC1*. We previously reported that GFP-AtCCC1 localises to the Golgi and TGN/EE when transiently expressed in *Nicotiana benthamiana* leaves (Henderson et al., 2015). However, other studies suggested a different localisation, so

further clarification of CCC1 subcellular localisation is needed (Chen et al., 2016b; Domingos et al., 2019).

Expression of *OsCCC1.1* was observed in almost all cell types, with particularly strong expression in root tips (Chen et al., 2016b), while reports on *AtCCC1* expression are somewhat contradictory. Promoter-GUS studies indicate expression is restricted to specific tissues, such as root stele or hydathodes and pollen (Colmenero-Flores et al., 2007), while RNA transcriptomic studies suggest expression occurs in other cell types such as root hairs (Lan et al., 2013). Loss of CCC1 function causes diverse defects in rice *Osccc1.1* and Arabidopsis *Atccc1* knockouts, while knockdown of the lowly expressed *Osccc1.2* did not lead to any obvious phenotypic alterations (Colmenero-Flores et al., 2007; Henderson et al., 2015; Chen et al., 2016b). The *Atccc1* phenotype includes a strongly reduced shoot and root growth, a bushy appearance due to a strong increase in axillary shoot outgrowth, frequent stem necrosis and very low fertility despite the formation of many siliques. Similarly, rice *Osccc1.1* has reduced height, low fertility and shows a reduced number of seeds per plant (Johnson et al., 2004; Colmenero-Flores et al., 2007; Henderson et al., 2015; Chen et al., 2016b).

Plant CCC1s have been suggested to improve tolerance to osmotic and salt stress (Colmenero-Flores et al., 2007; Wegner, 2014; Henderson et al., 2015; Chen et al., 2016b); however, the complexity of the knockout phenotypes under standard growth conditions suggests a core cellular role that leads to the many observed downstream effects. Very recently, a study revealed that loss of *AtCCC1* results in major changes in the cell wall, and a complex pathogen related phenotype, with *Atccc1* having a compromised defence to pathogens but displaying an enhanced response to non-pathogenic microbes (Han et al.,

2019). The different phenotypic defects of *ccc1* knockouts resemble those of other endomembrane transport knockouts combined, suggesting that these phenotypes might originate from the same upstream process.

Here, we provide evidence that AtCCC1 functions in the TGN/EE, when stably expressed in a native cell type, Arabidopsis root hair cells. We show that both Arabidopsis and rice CCC1 are important for root hair growth; and CCC1s are important for endomembrane trafficking, including trafficking of the auxin transporter PIN1 and the PM protein LTI6b. We observed seed coat defects in *Atccc1* and a complex role of AtCCC1 in osmoregulation, consistent with the modified delivery of proteins and cell wall material to the PM. We propose that CCC1 impacts these processes because it is the missing component of the ion regulating machinery of the TGN/EE.

Results

AtCCC1 *is expressed in the majority of cells.*

To clarify the tissue expression pattern of *AtCCC1*, we transformed Col-0 wildtype plants with a 2kb genomic DNA sequence upstream of the *AtCCC1* coding region driving the expression of nuclear localised triple Venus fluorochrome (a bright variant of YFP) or *GUS* (named *AtCCC1prom::Venus* and *AtCCC1prom::GUS*, respectively). Combined analysis of fluorescence and *GUS* expression revealed that *AtCCC1* is expressed in almost all cell types, similar to *OsCCC1.1* (Chen et al., 2016b), including all root cells, hypocotyl, leaf and stem epidermis, guard cells and trichomes, as well as mesophyll cells and most flower parts, with a particularly strong signal in stamen filaments (Fig. 1). *AtCCC1* promoter activity reported by fluorescence, or by GUS-activity, was slightly different despite use of the identical promoter sequence. For instance, fluorescence was detectable in root cortex and epidermis cells,

including root hairs, and in the gynoecium, while GUS staining did not indicate expression in these cells. This is likely due to the different sensitivities of the two methods.

ccc1 *knockout mutants have a reduced root hair length and tip growth rate*

As our expression analysis showed that *AtCCC1* is expressed in root hairs (Fig. 1), we examined whether root hair cells of the knockouts had an altered phenotype, and whether we could use this model cell type to investigate the role of CCC1. Characterisation of the knockouts showed that both *Atccc1* and *Osccc1.1* plants had a reduction in the overall length of their root hairs compared to control plants (Fig. 2); and a complete lack of collet hairs in *Atccc1*. Collet hairs are epidermal root hairs formed in some plant species in the transition zone between the root and the hypocotyl (Fig. 2, Sliwinska et al., 2015). *Atccc1* also had branching and bulging of root hairs, although, at a low frequency, and root hairs of the knockout mutants did not rupture (suppl. Fig. S1). *Atccc1* plants had a reduction in root epidermal cell length (Fig. 2), similar to what had been shown previously in *Osccc1.1* (Chen et al., 2016b); but different to *Osccc1.1*, root diameter was not decreased – instead, it was slightly larger in *Atccc1* (suppl. Fig. S1).

To investigate the cause of the reduced root hair length in *Atccc1*, the elongation rates of wildtype and *Atccc1* root hairs were measured using time lapse microscopy (suppl. Video 1-2). For this, roots were grown inside the media, directly in chambered cover slips. Measurements were taken from the beginning of root hair elongation, of root hairs that elongated beyond the initiation phase, until root hair growth ceased. This revealed that *Atccc1* root hairs were shorter because they grow at a reduced speed. The elongation rate of wildtype plants in our conditions was similar to what had previously been observed (Schoenaers et al., 2018). For wildtype, the average rate of root hair elongation between 50 and 100 minutes

after elongation initiated was 0.88 ± 0.27 µm min^{1-} while *Atccc1* root hairs elongated at half that speed, at 0.47 ± 0.08 µm min^{1-}, but for the same period of time, resulting in shorter root hairs (Fig. 2).

Atccc1 *plants show altered epidermal root cell specification*

Independent of the defect of root hair cell elongation, *Atccc1* plants also frequently developed ectopic root hairs (Fig. 1); these are root hairs that develop in cell files that usually exclusively contain atrichoblasts. In Arabidopsis, trichoblasts typically develop from an epidermal cell in contact with two cortical cells (Balcerowicz et al., 2015; Salazar-Henao et al., 2016). However, we could not observe defects in root cortex and epidermis cell arrangement (suppl. Fig. S1). The ectopic root hairs we observed in At*ccc1* are therefore the likely result of a defect in the root differentiation zone where cell types gain their specific cell identity, indicating that AtCCC1 has also a crucial role in root tip cells.

Atccc1 *localises to the endomembrane system in root hair cells*

We had previously localised AtCCC1 to the TGN/EE in transient expression assays in *N. benthamiana* (Henderson et al., 2015). In contrast, other studies have suggested that it might also localise to other membranes (Colmenero-Flores et al., 2007; Domingos et al., 2019), which has led to multiple interpretations of AtCCC1 function. Stable expression of GFP-AtCCC1 using the *EXP7* (*Expansin7*) root hair specific promoter revealed that the GFP signal was localised to internal organelles resembling components of the endomembrane system, similar to what we observed previously in *N. benthamiana* (Fig. 2) (Henderson et al., 2015). Time lapse imaging of the movement of GFP-AtCCC1 signal in root hairs and

trichoblasts was consistent with what could be expected for the TGN/EE (suppl. Videos V2 and V3). Co-staining with the lipid dye FM4-64 showed no PM localisation of AtCCC1, but co-localisation with FM4-64 in endosomes. Treatment with the trafficking inhibitor, brefeldin-A (BFA), caused the GFP signal to accumulate in the centre of BFA bodies, consistent with a TGN/EE localisation (Fig. 2). Expression of the GFP-AtCCC1 in the *Atccc1* knockout background complemented the short root hair phenotype and led to an increase of root hair length (Fig. 2), indicating that the tagged protein is functional. The formation of ectopic root hairs was not rescued in these plants (Fig. 2), consistent with our use of a root hair specific promoter to drive expression of this fluorescent construct; trichoblast specific expression of GFP-AtCCC1 was only induced after cell identity is conferred to epidermal cells.

After we had confirmed the subcellular localisation of AtCCC1 in Arabidopsis, we investigated if its loss impacts organelle ultrastructure. High-pressure freezing, freeze substitution, and transmission electron microscopy revealed that the lack of AtCCC1 does not lead to obvious morphological changes in the Golgi or TGN/EE ultrastructure, and the appearances of these organelles was similar between *Atccc1* mutants and wildtype (suppl. Fig S2).

Atccc1 *knockouts can withstand higher osmotic pressure before the onset of plasmolysis but do not have a higher cell sap osmolality*

Rice OsCCC1.1 has been suggested to be important for osmoregulation, and *Osccc1.1* plants were shown to have a lower cell sap osmolality (Chen et al., 2016b). We therefore tested if the endomembrane localised AtCCC1 could also be connected to tissue and cell osmoregulation. We first tested if *Atccc1* has a similar cell sap osmolality defect compared to

Osccc1.1, and found that *Atccc1* cell sap osmolality was not higher than wildtype, but showed a tendency to be lower (in *Atccc1-1*, while *Atccc1-2* was not significantly different from the wildtype, $p < 0.03$, and $p < 0.12$ for *Atccc1-1* and *Atccc1-2*, respectively, Fig. 3). These results and the endomembrane localisation of AtCCC1 suggest a role of CCC1s in osmoregulation that is different from directly mediating ions across the PM.

To test if the reduced osmolality of the *Atccc1* knockout cell sap impacts the capacity of the root cells to withstand osmotic stress, we tested the knockout under plasmolysis inducing conditions, using mannitol. Surprisingly, we found that for *Atccc1*, media with a higher (and not lower) osmotic strength was required to induce plasmolysis when compared to the wildtype (Fig. 3).

The PM marker GFP-LTI6b was used to visualise plasmolysis. At 250 mM mannitol, 71% of wildtype cells were plasmolysed, compared to only 23% of *Atccc1* cells (Fig. 3). This indicated that for the wildtype incipient plasmolysis (50% of cells are plasmolysed) occurs at ~233 mM Mannitol, and at ~278 mM mannitol for *Atccc1*, a 45 mM difference (Fig. 3, orange lines in graph). At 400 mM mannitol almost all cells were plasmolysed in both genotypes (Fig. 3). The lower sap osmolality, but the enhanced ability to withstand plasmolysis were seemingly contradictory results and suggested that cell features other than cell osmolality in the *ccc1* knockouts contribute to the observed phenotypes. It also suggested that the *ccc1* knockout mutants might perform better under osmotic stress, instead of worse.

Osmotic stress rescues root hair elongation defects in Atccc1 *and* Osccc1.1 *and knockouts are more tolerant to osmotic stress compared to wildtype*

As the knockout plants showed an increased capacity to withstand plasmolysis, we tested if the observed root phenotypes could be rescued by growing the plants on media with higher

osmotic strength. To assay this, plants were germinated and grown on media with osmotic stress caused by different concentrations of mannitol. *Atccc1* was able to germinate on media with much higher osmotic strength compared to the wildtype (suppl. Fig. S3). Additionally, collet hair formation was completely rescued in *Atccc1* by osmotic stress, back to control wildtype levels. We also confirmed these observations under sorbitol (suppl. Fig. S3). Osmotic stress is a component of salt stress, and we found that the *Atccc1* root hair phenotype is also rescued when plants are grown under increased NaCl (suppl. Fig. S3). This shows that the *ccc1* knockouts with a loss of CCC1 function are more tolerant to osmotic and salt stress in the cell-types examined and over the timeframes used in these experiments.

To test the effect of osmotic stress on root hair length, we utilised a combination of mannitol and low phosphate (Pi). We used these conditions as we found that osmotic stress on its own often leads to an increased percentage of root hairs that cease growing shortly after initiation, which strongly decreases the overall root hair length (Fig. 4), and because low Pi conditions are known to increase root hair formation of Arabidopsis and rice when grown *in vitro* (Bates and Lynch, 1996; Bhosale et al., 2018; Giri et al., 2018). We first assessed root hairs under low Pi only, so we were able to interpret the combined treatment. As expected, wildtype Arabidopsis plants showed a strong increase in root hair length under low Pi, while wildtype rice root hair length was similar under low Pi compared to control in our conditions. In *Atccc1*, however, no increase in root hair length could be observed in low Pi, this was similar to what we observed when we treated roots with IAA or 2,4-D (suppl. Fig. S4). Remarkably, the combination of low Pi and osmotic stress, however, completely rescued the *Atccc1* and *Osccc1.1* root hair phenotypes back to wildtype levels (Fig. 4).

We then investigated if the increased root hair length on osmotic stress was due to a prolonged root hair elongation period, or due to faster growth, using time lapse imaging of roots grown inside the media. When roots were grown inside the media (as opposed to on top

of the media for the above described assay), 150 mM mannitol alone was sufficient to rescue root hair growth (Fig. 4), indicating that the increase of external osmolality is responsible for *Atccc1* root hair rescue, independent of low Pi. Elongation speed measurements revealed that *Atccc1* root hair elongation rate was recovered under osmotic stress, with *Atccc1-1* root hairs elongating at a similar rate to wildtype root hairs, at 0.74 ± 0.43 and 0.82 ± 0.22 µm min^{1-} respectively between 50 and 100 minutes after elongation initiated (Fig. 4).

We also detected a decrease in elongation rate of wildtype root hairs grown under the osmotic stress conditions (0.74 ± 0.43 µm min^{1-}; Fig. 4) when compared to control (0.88 ± 0.27 µm min^{1-}; Fig. 2); and an increase in wildtype root hair elongation speed when grown under low Pi (1.02 ± 0.12 µm min^{1-}; Fig. 4). *Atccc1* elongation rate however, was reduced in low Pi (0.33 ± 0.21 µm min^{1-}; Fig. 4) when compared to control conditions (0.47 ± 0.08 µm min^{1-}; Fig. 2). Similar to osmotic stress alone, *Atccc1* root hair elongation rate increased to the growth rate of wildtype plants under low Pi when combined with osmotic stress (wildtype = 0.65 ± 0.20, *Atccc1*-1 = 0.68 ± 0.09 µm min^{1-}; Fig. 4). Therefore, moderately high external osmolality rescued the root hair elongation phenotype; however, it did not seem to rescue the development of ectopic root hairs (Fig. 4, suppl. Videos 5-10). Interestingly, we also noticed that a large proportion of the wildtype root hairs burst, when grown under low Pi and osmotic stress combined, while this did not happen as frequently in *Atccc1* (suppl. Videos 9-10).

Atccc1 *displays cell wall defects*

Root hair elongation depends on the correct synthesis and delivery of cell wall material to the tip and shank of the growing root hair. Defects in either the synthesis or delivery of cell wall material may be the cause of the root hair phenotype in *Atccc1*. This is supported by a very recent study showing major differences in monosaccharide composition in *Atccc1* compared

to the wildtype, suggesting that cell wall defects might contribute to the root hair defect in *Atccc1* (Han et al., 2019). A double knockout mutant of *Atccc1* and the *rhamnose synthase 1* (*rhm1-2*, also called *rol1-2*, Diet et al., 2006), a key enzyme involved in pectin formation, showed an extreme root hair phenotype, beyond a combination of those observed in *Atccc1* or *rhm1* alone (Fig. 5). This indicates AtCCC1 impacts the delivery of material to the cell wall.

As *Atccc1* showed the ability to germinate under higher osmotic stress than wildtype plants, we investigated the seedcoat. Seed coat defects and a weaker seed coat might contribute to the ability of *Atccc1* embryos to rupture the seed coat and germinate under extreme osmotic stress. Ruthenium red staining of the seed mucilage of imbibed seeds revealed a decreased, and irregularly distributed amount of mucilage in *Atccc1* (Fig. 5). The autofluorescence pattern of seed columella cells revealed that some columella cells formed normally in *Atccc1* while others did not, creating a patchwork appearance (Fig. 5).

Atccc1 *cells contain increased cytoplasmic material and an altered vacuolar morphology*

The multitude of different defects in *Atccc1* suggested that a fundamental cellular process is disrupted in *Atccc1*; we therefore investigated cell morphology and organelle dynamics in more detail. *Atccc1* root hairs showed the typical inverse fountain movement of the cytoplasm, similar to wildtype plants (Grierson et al., 2014; Balcerowicz et al., 2015). However, DIC images also revealed that the amount of cytoplasm was strongly increased in *Atccc1* (Fig. 6, suppl. Videos 11-13); which was accompanied by a change in vacuolar morphology (Fig. 6). To confirm the altered vacuolar morphology, the vacuole stain BCECF, together with the stably expressed TGN marker VHAa1-mRFP, was used to visualise the vacuole and the TGN/EE, respectively (Fig. 6) (Dettmer et al., 2006; Scheuring et al., 2015).

BCECF staining showed that the vacuolar occupancy of root hairs was decreased in *Atccc1*, with the TGN/EE-marker VHa1-mRFP present throughout the increased cytoplasmic space.

Atccc1 *root cells have a reduced rate of endocytosis, altered exocytosis and modified PIN1 localisation*

The increased volume of cytoplasmic material indicated alterations in the endomembrane system in *Atccc1*. We therefore measured rates of endo- and exocytosis in the mutant and wildtype, in cells close to the root tip, which are typically used to investigate endo- and exocytosis and in which *AtCCC1* is also expressed. Endocytosis was assayed by measuring the internalisation of the endocytic tracer dye, FM4-64. This was measured by taking a fluorescence intensity ratio of signal inside the cell *versus* at the PM, indicating the quantity of FM4-64 stained PM being internalised into the endomembrane system over a set time. As any differences in exocytic rates between wildtype and *Atccc1* would also alter the FM4-64 ratio, the trafficking inhibitor BFA was used (Richter et al., 2007; Teh and Moore, 2007). Only 10 minutes after combined treatment with FM4-64/BFA, *Atccc1* cells already showed a lower fluorescent ratio to wildtype indicating a decrease in the endocytosis of FM4-64 (Fig. 6). After 60 minutes of treatment (10 minutes with FM4-64/BFA, 50 minutes with BFA only), the fluorescent ratio was much lower in *Atccc1* than wildtype, indicating a large reduction the rate of endocytosis.

Exocytosis was assayed by first treating roots stably expressing either PIN1-GFP or the PM-marker GFP-LTI6b with BFA (Cutler et al., 2000; Benkova et al., 2003). BFA causes retention of the PIN1 and LTI6b within the endomembrane system, as it inhibits protein recycling. Upon BFA washout, recycling to the plasma membrane is resumed, and exocytosis rates can be compared. In the wildtype background, prior to BFA treatment, the initial ratio of

internal:PM fluorescence for both proteins, PIN1 and LTI6b, was very low, indicating that most of the proteins were at the PM (Fig. 6, Fig S5). This is in contrast to *Atccc1*, where the internal:PM fluorescence ratio was already very high before treatment, indicating a decreased percentage of PIN1 and LTI6b at the PM (Fig. 6, Fig S5). After 60 minutes of treatment with BFA, the GFP signal was internalised in all genotypes, however, as the cell-internal signal in *Atccc1* was already high before treatment, the impact of BFA was minimal (Fig. 6). As there is a substantial percentage of PIN1 and LTI6b protein inside the cells in *Atccc1* without treatment, it is difficult to estimate the rate of exocytosis in *Atccc1*. Yet, the altered subcellular distribution of the two primarily PM-localised proteins suggest a general defect with exocytosis in *Atccc1*.

Discussion

Here, we show the subcellular localisation of AtCCC1 in its native tissue, and can unequivocally confirm its localisation to endomembranes with a functional GFP-AtCCC1 construct that complements root hair length in the *Atccc1* knockout background (Fig. 2); no PM localisation was observed.

Our results also reveal that *ccc1* knockout plants perform better under higher external osmolality (Fig. 3; Fig. 4). The complementation of *Atccc1* and *Osccc1.1* root hair length under moderately high external osmolality suggests that CCC1s are either only required for normal cell elongation below a certain external osmotic threshold, or that loss of CCC1s improves the ability of the cells to grow in higher osmotic conditions. The lower cell sap osmolality in Arabidopsis and rice knockouts demonstrates that the complementation mechanism does not entail an increased accumulation of osmolytes. There is a regulatory connection between osmoregulation and cell wall properties, and *Atccc1* knockouts have been

shown to have an altered cell wall composition in addition to their defects in osmoregulation (Fig. 5; Han et al., 2019). Knockout mutants of proteins connected to cell wall-to-cell signalling, such as fer (loss of function of the receptor kinase FERONIA), have also been shown to be more tolerant to osmotic stress compared to wildtype (Chen et al., 2016a).

The ectopic root hair development in *Atccc1* suggests that AtCCC1 is involved in more than cell wall synthesis and secretion. The auxin transporter PIN1 showed an altered subcellular localisation pattern, and, similar to what is suggested for *nhx5 nhx6* and *kea4 kea5 kea6* (Dragwidge et al., 2018; Fan et al., 2018; Wang et al., 2019), defects in auxin distribution or signalling might contribute to some of the observed phenotypes in *Atccc1*, such as the bushy appearance of shoots.

Our results on the function and cellular role of CCC1 transporters in Arabidopsis and rice, together with previous phenotypic observations (Colmenero-Flores et al., 2007; Henderson et al., 2015; Chen et al., 2016b; Han et al., 2019), suggest that the complex phenotypes of the knockouts are most likely to originate from an impaired endomembrane trafficking system. Other TGN/EE localised transport proteins together with the V-type H^+-ATPase proton pump have been suggested to be critical for establishing optimal pH and ionic conditions in the TGN/EE, important for cargo delivery or pathogen resistance (Martinière et al., 2013; Shen et al., 2013; Guo et al., 2014; Luo et al., 2015). Currently, the model for ion and pH regulation consists of the V-H-ATPase, the cation proton antiporters NHX5, NHX6, KEA4, KEA5 and KEA6, and the chloride proton antiporter CLC-d (Guo et al., 2014; Sze and Chanroj, 2018; Zhu et al., 2018; Wang et al., 2019). It is suggested that the proton pump generates the H^+ gradient to establish the lower pH in the TGN/EE lumen compared to the cytosol, and that the ion proton antiporter contributes to fine-tuning the pH. This model lacks an ion efflux shunt that would be important to maintain ionic balance in the lumen. We therefore propose that

CCCs are candidates for the missing component in the pH and ionic condition establishing transport circuit in the TGN/EE (Fig. 7). Further investigation of the *Atccc1*, using pH and ionic sensors is now required to confirm this model.

Material and Methods

Plant material and growth conditions

Arabidopsis thaliana were all in the Columbia-0 (Col-0) background. Previously described T-DNA insertion lines in AT1G30450, *Atccc1-1* (SALK-048175) and *Atccc1-2* (SALK-145300) (Colmenero-Flores et al., 2007) were used in this study along with *rhm1-2* (= rol1-2, point mutation in AT1G78570, Diet et al., 2006). The *Osccc1.1* line was previously described, and has a point mutation in LOC_Os08g23440, is in the Japonica Nipponbare background, which was used as wildtype control (Chen et al., 2016b). *PIN1::PIN1-GFP*, *35S::VHAa1-RFP*, *35S::GFP-LTIB6* plant lines were previously described (Cutler et al., 2000; Benkova et al., 2003; Dettmer et al., 2006).

In general, Arabidopsis and rice were grown on media containing half strength Murashige and Skoog (1/2 MS) 0.1% sucrose, 0.6% phytagel, pH 5.6 with KOH. For the different treatments, 1/2 MS without Pi was used, 150 mM mannitol or a combination. Plants were sown on plates, incubated at 4°C for at least 2 days and subsequently grown vertically at 21°C and 19°C in 16 h light and 8 h dark, respectively. Plants were grown for different periods of time, as indicated below and stated in the figure legends.

Promoter activity analysis by GUS and Venus fluorescence

GUS staining was done according to (Jefferson et al., 1987). In summary, plants with the ages indicated in figure legend 1 were submerged in GUS-staining solution and stained for the times indicated in figure legend 1. Image of the entire rosette was captured with a Nikon digital camera, flower and inflorescence images with a Nikon SMZ25 stereo microscope. Fluorescence of the nuclear localised NLS-Venus was imaged in plants ranging from 5-8d to 8 weeks as indicated in figure legend 1. Excitation light wavelength was 514 nm, emission was detected at 540 nm, using either a Nikon A1R Confocal Laser-Scanning Microscope or an Olympus FV3000 Confocal Microscope.

GFP-AtCCC1 cloning and expression

For stable expression of AtCCC1 in root hairs, 1402 bp of the trichoblast specific promoter *EXP7* (Marquès-Bueno et al., 2016) was first amplified from Col-0 genomic DNA, using the primers EXP7pro-HindIII_F (*tatacAAGCTTATTACAAAGGGGAAATTTAGGT*) and EXP7pro-KpnI_R (*cttatGGTACCTCTAGCCTCTTTTTCTTTATTC*), following a Phusion® PCR protocol (NEB). PCR product and the binary plasmid pMDC43 were subsequently cut with the restriction enzymes HindIII-HF and KpnI-HF to remove the *2x35S* promoter, and the digestion reactions were purified using illustra™ GFX™ PCR DNA and Gel Band Purification kits. Fragment ligation was performed using T4 DNA Ligase protocol (NEB) at 16°C overnight. 2 µl of the ligation reaction was transformed into DB3.1 cells and after a sequencing verification, a plasmid was subsequently selected that showed the correct replacement of the *2x35* promoter with the *EXP7* promoter. *AtCCC1* CDS (with stop codon) was then shuttled into the pMDC43EXP7 using LR clonase II enzyme, which creates N-terminally GFP-tagged AtCCC1. Correct plasmids were transformed into *Agrobacterium*

tumefaciens, and heterozygous Arabidopsis plants (*Atccc1*$^{+/-}$) were floral dipped; as the homozygous *Atccc1* knockout does not support floral dipping well. Floral dipping was performed according to Clough and Bent (1998), and transformants were selected on 1/2 MS plates with no sucrose containing hygromycin for selection. *Atccc1* knockouts expressing the GFP were selected, and GFP fluorescence images show maximum intensity projections of stack image series, using GFP image setting as described in Henderson et al. (2015).

Root hair length, root hair elongation rate and cytoplasmic content

Light microscopy imaging of root hair length was performed using a Nikon SMZ25 stereo microscope with a 2x objective. For quantification of root hair length, images of roots were taken from above the maturation zone of 6 day old plants. Root length was measured using FIJI (Schindelin et al., 2012; Rueden et al., 2017).

For time lapse light microscopy of root hair elongation rate, plants were germinated within 2 mL of media placed in 1-well microscopy slides (Thermo Fisher) and grown vertically. Images of root hairs in the maturation zone were taken every 30 seconds for 6 hours using a Nikon Diaphot 300. For consistency, elongation rates of root hairs were only measured for root hairs where both initiation and cessation of growth could be observed in the time lapse. Analysis and creation of videos was performed using FIJI.

Cytoplasmic streaming in root hairs was imaged in 6 day old plants. Root hairs that were still elongating were selected from the maturation zone. Images were taken using DIC on a Nikon Ni-E microscope. Time lapses were taken with images every 2 seconds for 120 seconds.

Root morphology imaging

Root morphology images for epidermis cell length, ectopic root hairs and root hair position were taken at the same Nikon confocal, using 6 days old seedlings and root cell wall autoflorescence (excitation = 404 nm, emission = 425 - 475 nm).

Plasmolysis

Mannitol was used to induce plasmolysis of plants grown 6 d on 1/2 MS without mannitol. The mannitol concentration at which root cells plasmolyse was determined using the non-root hair cells of plants expressing the PM marker LTI6b-GFP. Plants were transferred from the growth media to a liquid 1/2 MS solution containing a specified concentration of mannitol 1 hour before counting. Cells were counted under a Nikon Ni-E light microscope. From each root, the plasmolysis state of 40 cells was assessed. Only cells past the maturation zone of the plant were observed.

Vacuolar morphology

Vacuole staining in 6 day old root hairs was performed using BCECF (Invitrogen) as previously described (Lofke et al., 2015). Briefly, plants were treated with 10 µM BCECF in liquid 1/2 MS with 0.02% pluronic acid (Invitrogen) for 1 h in the dark. Plants were then washed 1x with liquid 1/2 MS and Z-stacks were obtained of BCECF fluorescence (excitation = 488 nm, emission = 500 – 550 nm), imaged at the same Nikon confocal described above. Root hairs from the maturation zone were selected for imaging.

Seed coat staining and imaging

Seeds were stained with ruthenium red according to McFarlane et al. (2014), using the EDTA method. Seed coat autofluorescence (emission = 425-475 nm) was imaged using dry, untreated seeds. All seeds were imaged at a Nikon SMZ25 stereo microscope

Endo- and Exocytosis

Endocytosis was assayed in the root tips of 6 day old plants using the fluorescent membrane stain FM4-64 (excitation = 561 nm, emission = 570 – 620 nm) and the endomembrane trafficking inhibitor brefeldin A (BFA). Plants were either incubated in 1/2 MS containing 4 µM FM4-64 and 25 µM BFA in the dark for 10 minutes before imaging or for 10 minutes in 1/2 MS with 4 µM FM4-64 and 25 µM BFA in the dark before washing and incubating in 1/2 MS with 25 µM BFA for 50 minutes before imaging. A ratio of internal/PM signal was measured in imageJ by using the polygon selection tool to measure the mean grey value of the entire interior of the cell and divide this by the PM mean grey value, acquired using the segmented line tool (width 1).

Exocytosis was assayed in the root tips of 6 day old plants using PIN1-GFP in the stele or LTI6b-GFP in the epidermis. For the untreated image point, plants were taken directly off growth media and immediately imaged. Otherwise, plants were treated with 25 µM BFA for 60 minutes, at which point some plants were imaged. The rest were washed in liquid 1/2 MS and left to recover for 60 minutes in liquid 1/2 MS media before imaging. Signal internalisation was measured as described for endocytosis.

Acknowledgments

We thank Jian Feng Ma for kindly providing rice seeds; Christoph Ringli for providing the *rhm1* (*rol1-2*) seeds and Marina Oliva for providing PIN1::PIN1-GFP seeds. We thank Renée Philips and Marie Beillevert for assistance with lab and plant work; and Matthew Tucker for providing the 3xVenusNLS plasmid. We thank Adelaide Microscopy, especially Gwen Mayo and Jane Sibbons, for support with microscopy; and we thank the University of Melbourne Advanced Microscopy Facility where Electron microscopy was conducted. We thank the Adelaide plant accelerator team for assistance with rice growth facilities; and Steve Tyerman and Philip Brewer for helpful discussions. HEM is supported in part by funding from the CRC program as the Canada Research Chair in Plant Cell Biology. We thank the Australian Research Council for funding this work through DE170100054 to HEM, FT130100709 and CE140100008 to M.G., and DE160100804 to S.W.

Author contributions

SW led the project; DWM, MG and SW designed experiments; DWM and SW conducted most experiments with contribution from YQ and AS; HEM conducted TEM imaging and gave advice on endo- and exocytosis experiments; DWM, MG and SW wrote the paper, HEM and YQ commented on the paper.

References

Balcerowicz, D., Schoenaers, S., and Vissenberg, K. (2015). Cell fate determination and the switch from diffuse growth to planar polarity in *Arabidopsis* root epidermal cells. Frontiers in Plant Science **6,** 1163.

Bassil, E., and Blumwald, E. (2014). The ins and outs of intracellular ion homeostasis: NHX-type cation/H^+ transporters. Current Opinion in Plant Biology **22,** 1-6.

Bassil, E., Ohto, M.-a., Esumi, T., Tajima, H., Zhu, Z., Cagnac, O., Belmonte, M., Peleg, Z., Yamaguchi, T., and Blumwald, E. (2011). The Arabidopsis intracellular Na^+/H^+ antiporters NHX5 and NHX6 are endosome associated and necessary for plant growth and development. Plant Cell **23,** 224-239.

Bates, T., and Lynch, J.P. (1996). Stimulation of root hair elongation in *Arabidopsis thaliana* by low phosphorus availability. Plant physiology **19,** 529-538.

Benkova, E., Michniewicz, M., Sauer, M., Teichmann, T., Seifertova, D., Jurgens, G., and Friml, J. (2003). Local, efflux-dependent auxin gradients as a common module for plant organ formation. Cell **115,** 591-602.

Bhosale, R., Giri, J., Pandey, B.K., Giehl, R.F.H., Hartmann, A., Traini, R., Truskina, J., Leftley, N., Hanlon, M., Swarup, K., Rashed, A., Voß, U., Alonso, J., Stepanova, A., Yun, J., Ljung, K., Brown, K.M., Lynch, J.P., Dolan, L., and Vernoux, T. (2018). A mechanistic framework for auxin dependent *Arabidopsis* root hair elongation to low external phosphate. Nature Communications **9,** 1409.

Chen, J., Yu, F., Liu, Y., Du, C., Li, X., Zhu, S., Wang, X., Lan, W., Rodriguez, P.L., Liu, X., Li, D., Chen, L., and Luan, S. (2016a). FERONIA interacts with ABI2-type phosphatases to facilitate signaling cross-talk between abscisic acid and RALF peptide in *Arabidopsis*. Proceedings of the National Academy of Sciences **113,** E5519-5527.

Chen, Z.C., Yamaji, N., Fujii-Kashino, M., and Ma, J.F. (2016b). A cation-chloride cotransporter gene Is required for cell elongation and osmoregulation in rice. Plant Physiology **171,** 494-507.

Clough, S.J., and Bent, A.F. (1998). Floral dip: a simplified method for *Agrobacterium*-mediated transformation of *Arabidopsis thaliana*. Plant Journal **16,** 735-743.

Colmenero-Flores, J.M., Martínez, G., Gamba, G., Vázquez, N., Iglesias, D.J., Brumós, J., and Talón, M. (2007). Identification and functional characterization of cation–chloride cotransporters in plants. Plant Journal **50,** 278-292.

Cutler, S., R. , Ehrhardt, D., W., Griffitts, J., S., and Somerville, C., R. (2000). Random GFP::cDNA fusions enable visualization of subcellular structures in cells of *Arabidopsis* at a high frequency. Proceedings of the National Academy of Sciences **97,** 3718-3723.

Dettmer, J., Hong-Hermesdorf, A., Stierhof, Y.-D., and Schumacher, K. (2006). Vacuolar H^+-ATPase activity is required for endocytic and secretory trafficking in *Arabidopsis*. Plant Cell **18,** 715-730.

Diet, A., Link, B., Seifert, G.J., Schellenberg, B., Wagner, U., Pauly, M., Reiter, W.-D., and Ringli, C. (2006). The *Arabidopsis* root hair cell wall formation mutant *lrx1* is suppressed by mutations in the *RHM1* gene encoding a UDP-L-rhamnose synthase. Plant Cell **18,** 1630-1641.

Domingos, P., Dias, P.N., Tavares, B., Portes, M.T., Wudick, M.M., Konrad, K.R., Gilliham, M., Bicho, A., and Feijó, J.A. (2019). Molecular and electrophysiological characterization of anion transport in *Arabidopsis thaliana* pollen reveals regulatory roles for pH, $Ca2^+$ and GABA. New Phytologist **223,** 1353-1371.

Dragwidge, J.M., Ford, B.A., Ashnest, J.R., Das, P., and Gendall, A.R. (2018). Two endosomal NHX-Type Na^+/H^+ antiporters are involved in auxin-mediated development in *Arabidopsis thaliana*. Plant and Cell Physiology **59,** 1660-1669.

Fan, L., Zhao, L., Hu, W., Li, W., Novák, O., Strnad, M., Simon, S., Friml, J., Shen, J., Jiang, L., and Qiu, Q.S. (2018). $Na^+,K^+/H^+$ antiporters regulate the pH of endoplasmic reticulum and auxin-mediated development. Plant, Cell & Environment **41,** 850-864.

Gendre, D., McFarlane, H.E., Johnson, E., Mouille, G., Sjodin, A., Oh, J., Levesque-Tremblay, G., Watanabe, Y., Samuels, L., and Bhalerao, R.P. (2013). *Trans*-Golgi Network localized ECHIDNA/Ypt interacting protein complex is required for the secretion of cell wall polysaccharides in *Arabidopsis*. Plant Cell **25,** 2633-2646.

Gendre, D., Oh, J., Boutté, Y., Best, J., G., Samuels, L., Nilsson, R., Uemura, T., Marchant, A., J. Bennett, M., Grebe, M., and P. Bhalerao, R. (2011). Conserved *Arabidopsis* ECHIDNA protein mediates *trans*–Golgi-network trafficking and cell elongation. Proceedings of the National Academy of Sciences **108,** 8048-8053.

Giri, J., Bhosale, R., Huang, G., K. Pandey, B., Parker, H., Zappala, S., Yang, J., Dievart, A., Bureau, C., Ljung, K., Price, A., Rose, T., Larrieu, A., and Mairhofer, S. (2018). Rice auxin influx carrier OsAUX1 facilitates root hair elongation in response to low external phosphate. Nature Communications **9,** 1408.

Grierson, C., Nielsen, E., Ketelaarc, T., and Schiefelbein, J. (2014). Root hairs. Arabidopsis Book **12,** e0172.

Guan, R., Qu, Y., Guo, Y., Yu, L., Liu, Y., Jiang, J., Chen, J., Ren, Y., Liu, G., Tian, L., Jin, L., Liu, Z., Hong, H., Chang, R., Gilliham, M., and Qiu, L. (2014). Salinity tolerance in soybean is modulated by natural variation in *GmSALT3*. Plant Journal **80,** 937-950.

Guo, W., Zuo, Z., Cheng, X., Sun, J., Li, H., Li, L., and Qiu, J.-L. (2014). The chloride channel family gene *CLCd* negatively regulates pathogen-associated molecular pattern (PAMP)-triggered immunity in *Arabidopsis*. Journal of Experimental Botany **65,** 1205-1215.

Han, B., Jiang, Y., Cui, G., Mi, J., Roelfsema, R., Mouille, G., Sechet, J., Al-Babili, S., Aranda, M., and Hirt, H. (2019). CATION-CHLORIDE CO-TRANSPORTER 1 (CCC1) mediates plant resistance against *Pseudomonas syringae*. Plant Physiology.

Henderson, S., Wege, S., and Gilliham, M. (2018). Plant cation-chloride cotransporters (CCC): evolutionary origins and functional insights. International Journal of Molecular Sciences **19,** 492.

Henderson, S.W., Wege, S., Qiu, J., Blackmore, D.H., Walker, A.R., Tyerman, S.D., Walker, R.R., and Gilliham, M. (2015). Grapevine and Arabidopsis cation-chloride cotransporters localize to the Golgi and trans-Golgi network and indirectly influence long-distance ion transport and plant salt tolerance. Plant Physiology **169,** 2215-2229.

Jefferson, R.A., Kavanagh, T.A., and Bevan, M.W. (1987). GUS fusions: beta-glucuronidase as a sensitive and versatile gene fusion marker in higher plants. EMBO Journal **6,** 3901-3907.

Jentsch, T., and Pusch, M. (2018). CLC chloride channels and transporters: structure, function, physiology, and disease. Physiological Reviews **98,** 1493-1590.

Johnson, M., Zhou, Q., and Smith, E. (2004). Arabidopsis *hapless* mutations define essential gametophytic functions. Genetics **168,** 971-982.

Lan, P., Li, W., Lin, W.-D., Santi, S., and Schmidt, W. (2013). Mapping gene activity of *Arabidopsis* root hairs. Genome biology **14,** R67.

Liu, S., Chang, S., Han, B., Xu, L., Zhang, M., Zhao, C., Yang, W., Wang, F., Li, J., Delpire, E., Ye, S., Bai, X.-C., and Guo, J. (2019). Cryo-EM structures of the human cation-chloride cotransporter KCC1. Science **366,** 505-508.

Liu, Y., Yu, L., Qu, Y., Chen, J., Liu, X., Hong, H., Liu, Z., Chang, R., Gilliham, M., Qiu, L., and Guan, R. (2016). GmSALT3, which confers improved soybean salt tolerance in the field, increases leaf Cl^- exclusion prior to Na^+ exclusion but does not improve early vigor under salinity. Frontiers in Plant Science **7,** 1485.

Lofke, C., Dunser, K., Scheuring, D., and Kleine-Vehn, J. (2015). Auxin regulates SNARE-dependent vacuolar morphology restricting cell size. eLife **4,** e05868.

Luo, Y., Scholl, S., Doering, A., Zhang, Y., Irani, N.G., Rubbo, S.D., Neumetzler, L., Krishnamoorthy, P., Van Houtte, I., Mylle, E., Bischoff, V., Vernhettes, S., Winne, J., Friml, J., Stierhof, Y.-D., Schumacher, K., Persson, S., and Russinova, E. (2015). V-ATPase-activity in the TGN/EE is required for exocytosis and recycling in *Arabidopsis*. Nature Plants **1,** 15094.

Maresova, L., and Sychrova, H. (2005). Physiological characterization of *Saccharomyces cerevisiae kha1* deletion mutants. Molecular Microbiology **55,** 588-600.

Marquès-Bueno, M.M., Morao, A.K., Cayrel, A., Platre, M.P., Barberon, M., Caillieux, E., Colot, V., Jaillais, Y., Roudier, F., and Vert, G. (2016). A versatile Multisite Gateway-compatible promoter and transgenic line collection for cell type-specific functional genomics in Arabidopsis. Plant Journal **85,** 320-333.

Martinière, A., Bassil, E., Jublanc, E., Alcon, C., Reguera, M., Sentenac, H., Blumwald, E., and Paris, N. (2013). In vivo intracellular pH measurements in tobacco and *Arabidopsis* reveal an unexpected pH gradient in the endomembrane system. Plant Cell **25,** 4028-4043.

McFarlane, H., Gendre, D., and Western, T. (2014). Seed coat ruthenium red staining assay. Bio-Protocol **4**.

Padmanaban, S., Chanroj, S., Kwak, J., Li, X., Ward, J., and Sze, H. (2007). Participation of endomembrane cation/H^+ exchanger AtCHX20 in osmoregulation of guard cells. Plant Physiology **144,** 82-93.

Ravikumar, R., Kalbfuß, N., Gendre, D., Steiner, A., Altmann, M., Altmann, S., Rybak, K., Edelmann, H., Stephan, F., Lampe, M., Facher, E., Wanner, G., Falter-Braun, P., Bhalerao, R.P., and Assaad, F.F. (2018). Independent yet overlapping pathways ensure the robustness and responsiveness of trans-Golgi network functions in *Arabidopsis*. Development **145**.

Richter, S., Geldner, N., Schrader, J., Wolters, H., Stierhof, Y.-D., Rios, G., Koncz, C., Robinson, D., G., and Jürgens, G. (2007). Functional diversification of closely related ARF-GEFs in protein secretion and recycling. Nature **448,** 488-492.

Rueden, C.T., Schindelin, J., Hiner, M.C., Dezonia, B., Walter, A.E., Arena, E., and Eliceiri, K. (2017). ImageJ2: ImageJ for the next generation of scientific image data. BMC Bioinformatics **18,** 529.

Salazar-Henao, J., Velez-Bermudez, I., and Schmidt, W. (2016). The regulation and plasticity of root hair patterning and morphogenesis. Development **143,** 1848-1858.

Scheuring, D., Schöller, M., Kleine-Vehn, J., and Löfke, C. (2015). Vacuolar staining methods in plant cells. Methods in Molecular Biology **1242,** 83-92.

Schindelin, J., Arganda-Carreras, I., Frise, E., Kaynig, V., Longair, M., Pietzsch, T., Preibisch, S., Rueden, C., Saalfeld, S., Schmid, B., JTinevez, e.-Y., White, D.J., Hartenstein, V., Eliceiri, K., Tomancak, P., and Cardona, A. (2012). Fiji: an open-source platform for biological-image analysis. Nature Methods **9,** 676-682.

Schoenaers, S., Balcerowicz, D., Breen, G., Hill, K., Zdanio, M., Mouille, G., Holman, T.J., Oh, J., Wilson, M.H., Nikonorova, N., Vu, L.D., De Smet, I., Swarup, R., De Vos, W.H., Pintelon, I., Adriaensen, D., Grierson, C., Bennett, M.J., and Vissenberg, K. (2018). The auxin-regulated CrRLK1L kinase *ERULUS* controls cell wall composition during root hair tip growth. Current Biology **28,** 722-732.

Shen, J., Zeng, Y., Zhuang, X., Sun, L., Yao, X., Pimpl, P., and Jiang, L. (2013). Organelle pH in the *Arabidopsis* endomembrane system. Molecular Plant **6,** 1419-1437.

Sliwinska, E., Mathur, J., and Bewley, J.D. (2015). On the relationship between endoreduplication and collet hair initiation and tip growth, as determined using six

Arabidopsis thaliana root-hair mutants. Journal of Experimental Botany **66,** 3285-3295.

Sze, H., and Chanroj, S. (2018). Plant endomembrane dynamics: studies of K^+/H^+ antiporters provide insights on the effects of pH and ion homeostasis. Plant Physiology **177,** 875-895.

Sze, H., Padmanaban, S., Cellier, F., Honys, D., Cheng, N.-H., Bock, K.W., Conejero, G., Li, X., Twell, D., Ward, J.M., and Hirschi, K.D. (2004). Expression patterns of a novel *AtCHX* gene family highlight potential roles in osmotic adjustment and K^+ homeostasis in pollen development. Plant Physiology **136,** 2532-2547.

Teh, O.-K., and Moore, I. (2007). An ARF-GEF acting at the Golgi and in selective endocytosis in polarized plant cells. Nature **448,** 493-496.

Wang, Y., Tang, R.-J., Yang, X., Zheng, X., Shao, Q., Tang, Q.-L., Fu, A., and Luan, S. (2019). Golgi-localized cation/proton exchangers regulate ionic homeostasis and skotomorphogenesis in *Arabidopsis*. Plant, Cell & Enviroment **42,** 673-687.

Wegner, L.H. (2014). Root pressure and beyond: energetically uphill water transport into xylem vessels? Journal of Experimental Botany **65,** 381-393.

Zhu, X., Pan, T., Zhang, X., Fan, L., Quintero, F.J., Zhao, H., Su, X., Li, X., Villalta, I., Mendoza, I., Shen, J., Jiang, L., Pardo, J.M., and Qiu, Q.-S. (2018). K^+ Efflux Antiporters 4, 5, and 6 mediate pH and K^+ homeostasis in endomembrane compartments. Plant Physiology **178,** 1657-1678.

Figure legends

Figure 1: *AtCCC1* is expressed in the majority of cell types. Expression of either 3xVenus-NLS (bright YFP variant with a nuclear localisation signal) or β-Glucuronidase (blue GUS

676 staining). A-H) 3xVenusNLS expression indicating promoter activity in all root cells, including
677 the root tip and root hairs, and hypocotyl, leaf cells including trichomes and guard cells, as
678 well as stigma and stamen tissue. I-M) GUS staining indicating promoter activity
679 predominantly in younger leaves, floral stem, stamen stigma and root stele. Scale bars are 50
680 µm (images A-B, G), 100 µm (images C-D, H, J), 5 µm (image E), 20 µm (image F), 5 mm
681 (image I), 200 µm (images K, M) and 1000 µm (image L).

682

683 **Figure 2: CCC1s are important for root hair formation and exclusively localise to**
684 **endomembranes.** A-C) Arabidopsis and rice *ccc1* knockouts have shorter root hairs. D)
685 *Atccc1* does not develop collet hairs and E-F) epidermal cells are shorter in *Atccc1*. G) *Atccc1*
686 root hairs elongate slower (see also suppl. videos 1-2) and H) and Atccc1 develops ectopic
687 root hairs, trichoblast cell files indicated with green line, atrichoblast cell files with blue line.
688 I-K) Stably expressed GFP-AtCCC1 (green) localises to highly mobile endomembrane
689 structures in root hairs (see also suppl. videos 3-4), which co-localise with endosomes
690 stained with FM4-64 (magenta), but not the plasma membrane; GFP and FM4-64 signals co-
691 localise in BFA bodies. L) Expression of GFP-AtCCC1 complements root hair length in the
692 *Atccc1* background. Scale bars = 200 µm (images A, L), 500 µm (image D), 50 µm (images E,
693 H) and 10 µm (images I-K). n >900 (B), >200 (C), = 98-300 (F) and 7-10 (G). Student t-tests
694 comparing *Atccc1* to wildtype.

695

696 **Figure 3: *Atccc1* knockouts can withstand higher osmotic pressure before onset of**
697 **plasmolysis but do not have a higher root cells sap osmolality.** A) A higher osmotic strength

698 is required for incipient plasmolysis onset for *Atccc1* compared to wildtype plants, indicated
699 as orange lines for 50% cell plasmolysed. B) Example images of wildtype and *Atccc1* plants
700 expressing the plasma membrane marker LTI6b, which were exposed to osmotic shocks of
701 either 200 or 250 mM mannitol. Scale bars are 20 mm. n = 11-23 plants, 40 cells per plant,
702 student t-test comparing *Atccc1* and wildtype. C) Cell sap osmolality of whole root cell sap is
703 not higher in *Atccc1*, with values indicating a lower osmolality in *Atccc1-1* ($p<0.03$) and a
704 similar osmolality in *Atccc1-2* ($p<0.12$) when compared to wildtype. n = 9-10, student t-test
705 comparing *Atccc1* to wildtype.

706

707 **Figure 4: Osmotic stress rescued the *Atccc1* short root hair phenotype.** A-D) Both, rice
708 *Osccc1.1* and Arabidopsis *Atccc1* root hair length can be rescued by growing plants on media
709 with higher osmotic strength, combined with low Pi to induce root hair formation; plants
710 grown on top of solid media). E-G) Root hair elongation speed is increased to wildtype levels
711 when *Atccc1* plants are grown inside solid media with high mannitol; duration of root hair
712 elongation is increased in both, Col-0 wildtype and *Atccc1* under low Pi and mannitol. Scale
713 bars = 50 µm (image A), 100 µm (image C), n >600 (B), >200 (D), = 6-13 (E-G). Student t-test
714 comparing *Atccc1* to wildtype with $p < 0.001$. See also suppl. videos 5-10.

715

716 **Figure 5: Loss of *Atccc1* impacts the cell wall.** A) A double mutant of the *Rhamnose Synthase*
717 *1* (*rhm1-2*) and *Atccc1* showed an extremely severe root hair phenotype, beyond the
718 additive effects of either single knockout. B-C) Imbibed *Atccc1* seeds have reduced mucilage,
719 seed mucilage stained with ruthenium red. Scale bars = 100 µm, n = 41-43, student t-test D)

720 Seed coat columella cells are irregularly developed in *Atccc1*, shown by autofluorescence
721 (left panel) and stereo microscopy (right panel), scale bars = 100 µm.

722

723 **Figure 6: AtCCC1 is important for endomembrane trafficking.** A) DIC imaging of root hairs
724 shows strongly increased cytoplasm in *Atccc1* compared to Col-0 wildtype (see also suppl.
725 videos 11-13). Scale bars = 10 µm. B) BCECF staining of the vacuole (blue) in plants
726 expressing the TGN/EE marker VHAa1-mRFP (yellow) showing altered vacuolar morphology
727 in *Atccc1*. Scale bars = 5 µm. C-D) Endocytosis rate is reduced in *Atccc1*, C) Col-0 and *Atccc1*
728 root tip cells, stained with FM4-64 (red), and treated with BFA for 10 min or 60 min, D)
729 fluorescent ratio of plasma membrane to cell internal fluorescence. Scale bars = 10 µm, n =
730 56-89, students t-test comparing *Atccc1* and wildtype. E-F) Localisation pattern of auxin
731 transporter PIN1 is altered in *Atccc1*. E) Col-0 wildtype and *Atccc1* plants stably expressing
732 PIN1-GFP (green), expression driven by *PIN1* promoter. *Atccc1* plants showing reduced
733 plasma membrane localisation of PIN1-GFP and a reduced reaction to BFA treatment. Scale
734 bars = 10 µm, n = 13-27, students t-test comparing *Atccc1* and wildtype.

735

736 **Figure 7: Proposed model of ion and pH regulation in the TGN/EE, with CCC as the missing**
737 **component.** The V-ATPase proton pump, the cation-proton exchangers NHX5, NHX6, KEA4,
738 KEA5 and KEA6 and the anion proton exchanger CLC-d have been previously shown or
739 proposed to be important for pH regulation in the TGN/EE lumen (Sze and Chanroj, 2018).
740 CCC1s are candidates for providing an electroneutral ion shunt, completing the regulatory
741 transport circuit.

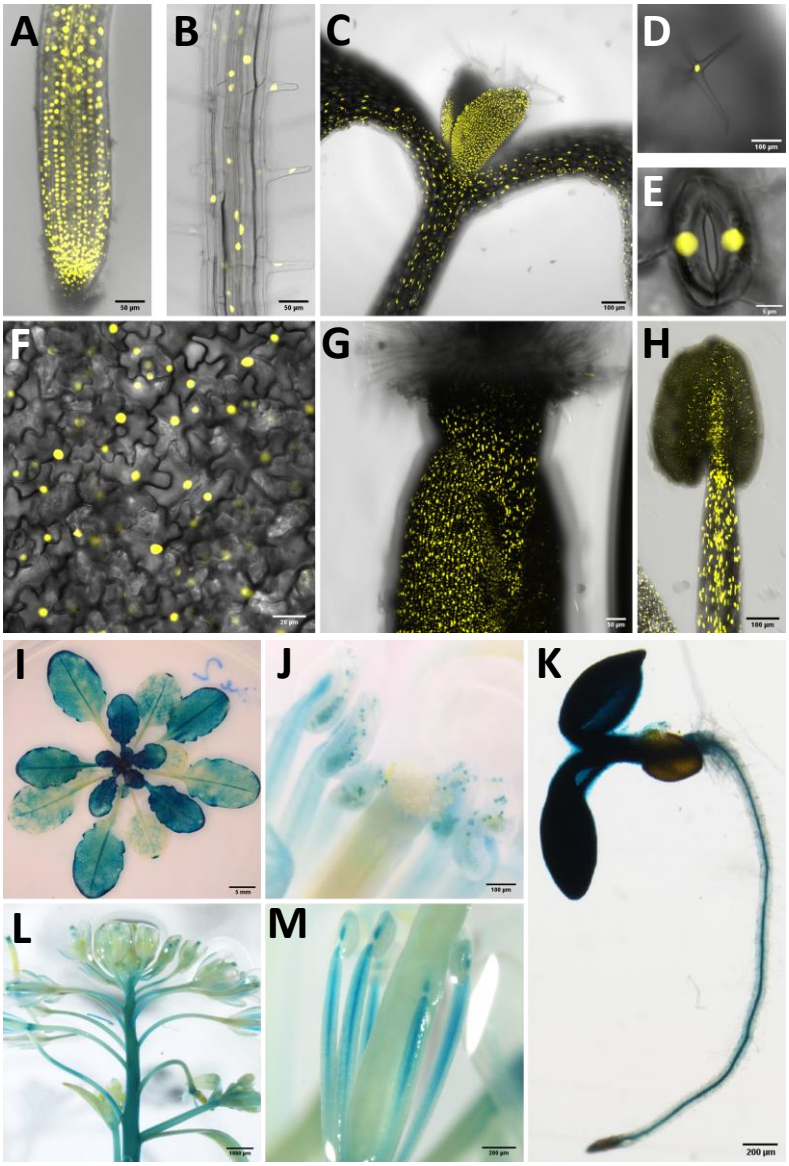

Figure 1: *AtCCC1* is expressed in the majority of cell types. Expression of either 3xVenus-NLS (bright YFP variant with a nuclear localisation signal) or β-Glucuronidase (blue GUS staining). A-H) 3xVenusNLS expression indicating promoter activity in all root cells, including the root tip and root hairs, and hypocotyl, leaf cells including trichomes and guard cells, as well as stigma and stamen tissue. I-M) GUS staining indicating promoter activity predominantly in younger leaves, floral stem, stamen stigma and root stele. Scale bars are 50 µm (images A-B, G), 100 µm (images C-D, H, J), 5 µm (image E), 20 µm (image F), 5 mm (image I), 200 µm (images K, M) and 1000 µm (image L).

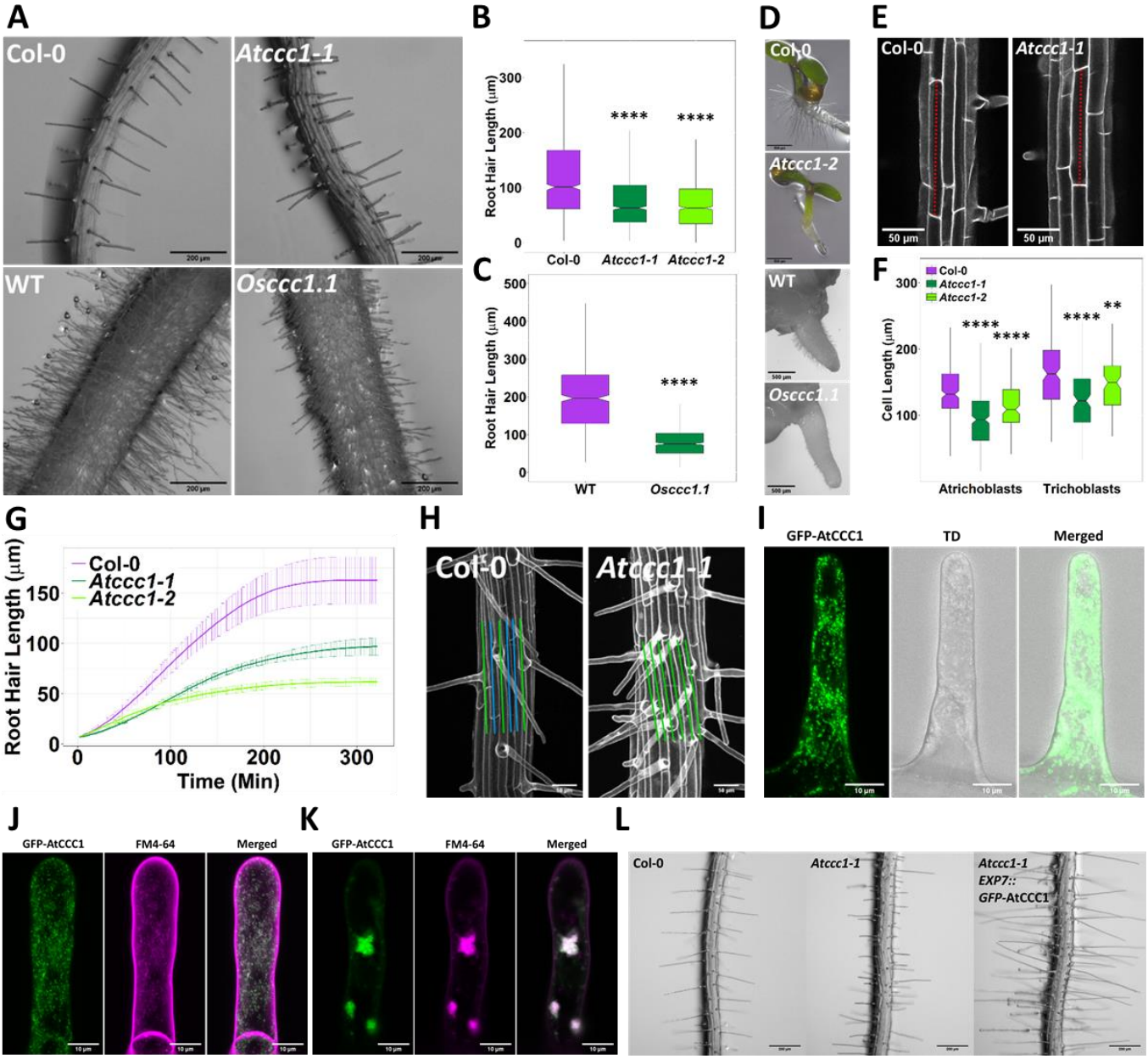

Figure 2: CCC1s are important for root hair formation and exclusively localise to endomembranes. A-C) Arabidopsis and rice *ccc1* knockouts have shorter root hairs. D) *Atccc1* does not develop collet hairs and E-F) epidermal cells are shorter in *Atccc1*. G) *Atccc1* root hairs elongate slower (see also suppl. videos 1-2) and H) and Atccc1 develops ectopic root hairs, trichoblast cell files indicated with green line, atrichoblast cell files with blue line. I-K) Stably expressed GFP-AtCCC1 (green) localises to highly mobile endomembrane structures in root hairs (see also suppl. videos 3-4), which co-localise with endosomes stained with FM4-64 (magenta), but not the plasma membrane; GFP and FM4-64 signals co-localise in BFA bodies. L) Expression of GFP-AtCCC1 complements root hair length in the *Atccc1* background. Scale bars = 200 µm (images A, L), 500 µm (image D), 50 µm (images E, H) and 10 µm (images I-K). n >900 (B), >200 (C), = 98-300 (F) and 7-10 (G). Student t-tests comparing *Atccc1* to wildtype.

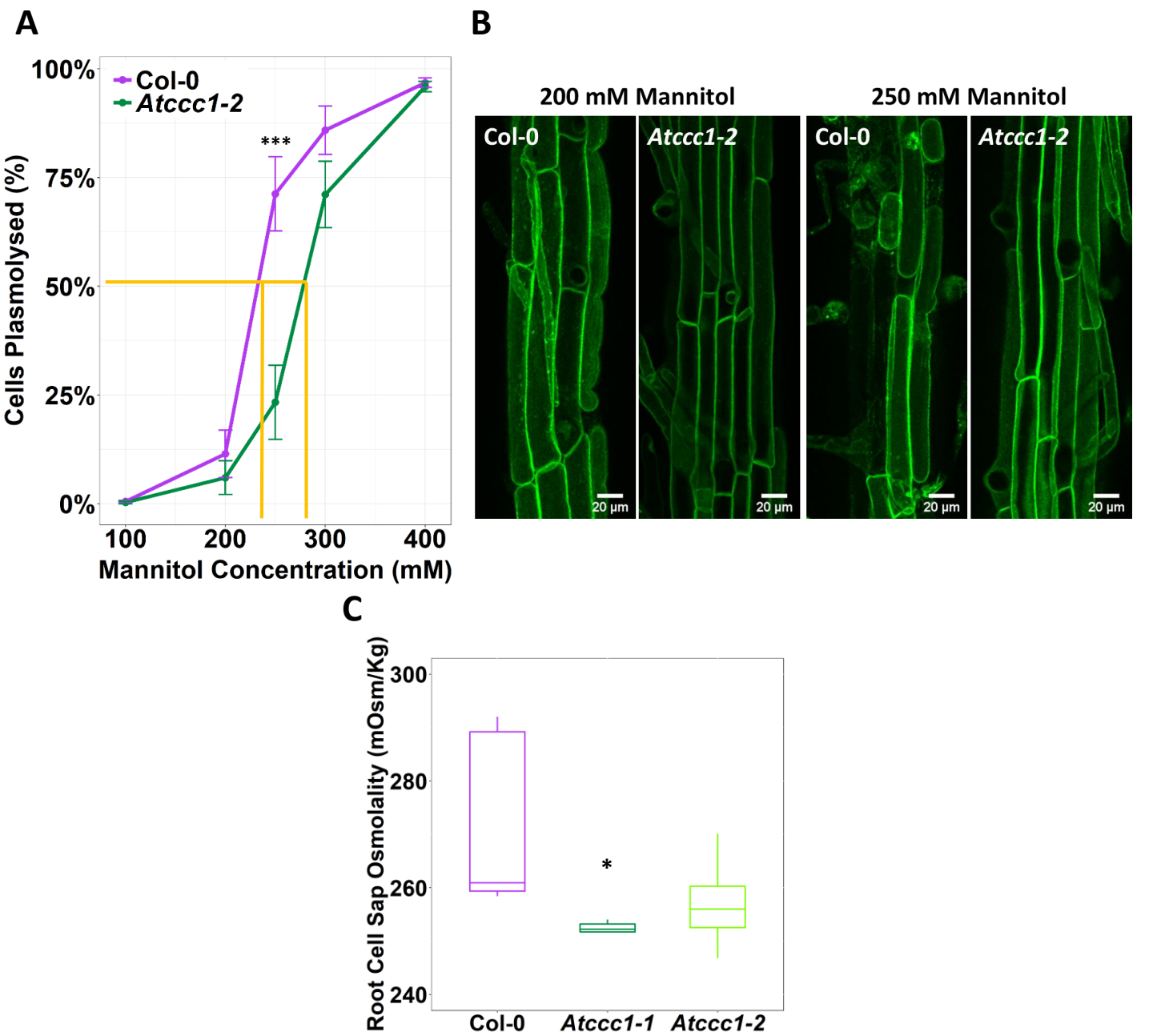

Figure 3: *Atccc1* knockouts can withstand higher osmotic pressure before onset of plasmolysis but do not have a higher root cells sap osmolality. A) A higher osmotic strength is required for incipient plasmolysis onset for *Atccc1* compared to wildtype plants, indicated as orange lines for 50% cell plasmolysed. B) Example images of wildtype and *Atccc1* plants expressing the plasma membrane marker LTI6b, which were exposed to osmotic shocks of either 200 or 250 mM mannitol. Scale bars are 20 µm. n = 11-23 plants, 40 cells per plant, student t-test comparing *Atccc1* and wildtype. C) Cell sap osmolality of whole root cell sap is not higher in *Atccc1*, with values indicating a lower osmolality in *Atccc1-1* ($p<0.03$) and a similar osmolality in *Atccc1-2* ($p<0.12$) when compared to wildtype. n = 9-10, student t-test comparing *Atccc1* to wildtype.

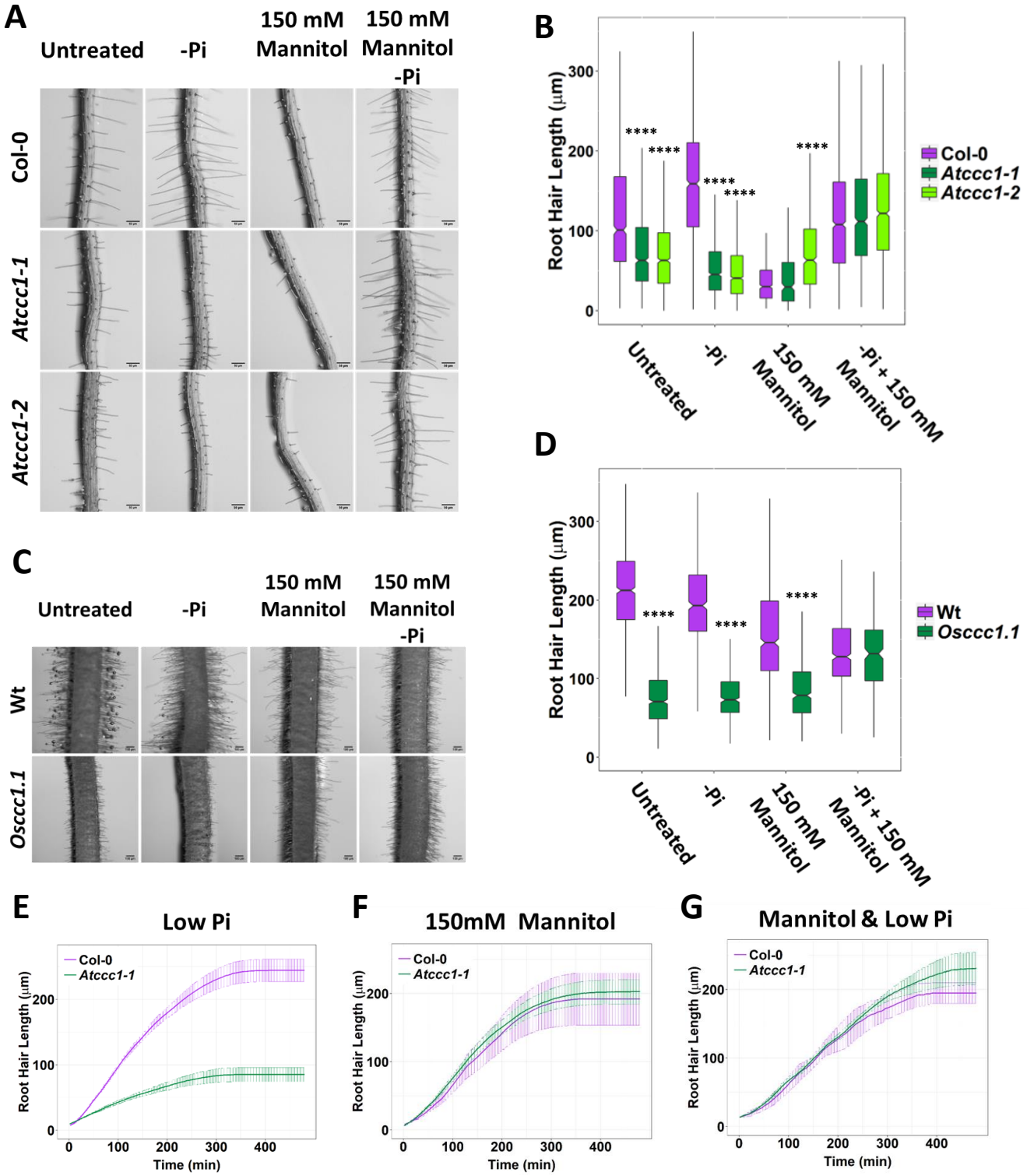

Figure 4: Osmotic stress rescued the *Atccc1* short root hair phenotype. A-D) Both, rice *Osccc1.1* and Arabidopsis *Atccc1* root hair length can be rescued by growing plants on media with higher osmotic strength, combined with low Pi to induce root hair formation; plants grown on top of solid media). E-G) Root hair elongation speed is increased to wildtype levels when *Atccc1* plants are grown inside solid media with high mannitol; duration of root hair elongation is increased in both, Col-0 wildtype and *Atccc1* under low Pi and mannitol. Scale bars = 50 µm (image A), 100 µm (image C), n >600 (B), >200 (D), = 6-13 (E-G). Student t-test comparing *Atccc1* to wildtype with $p < 0.001$. See also suppl. videos 5-10.

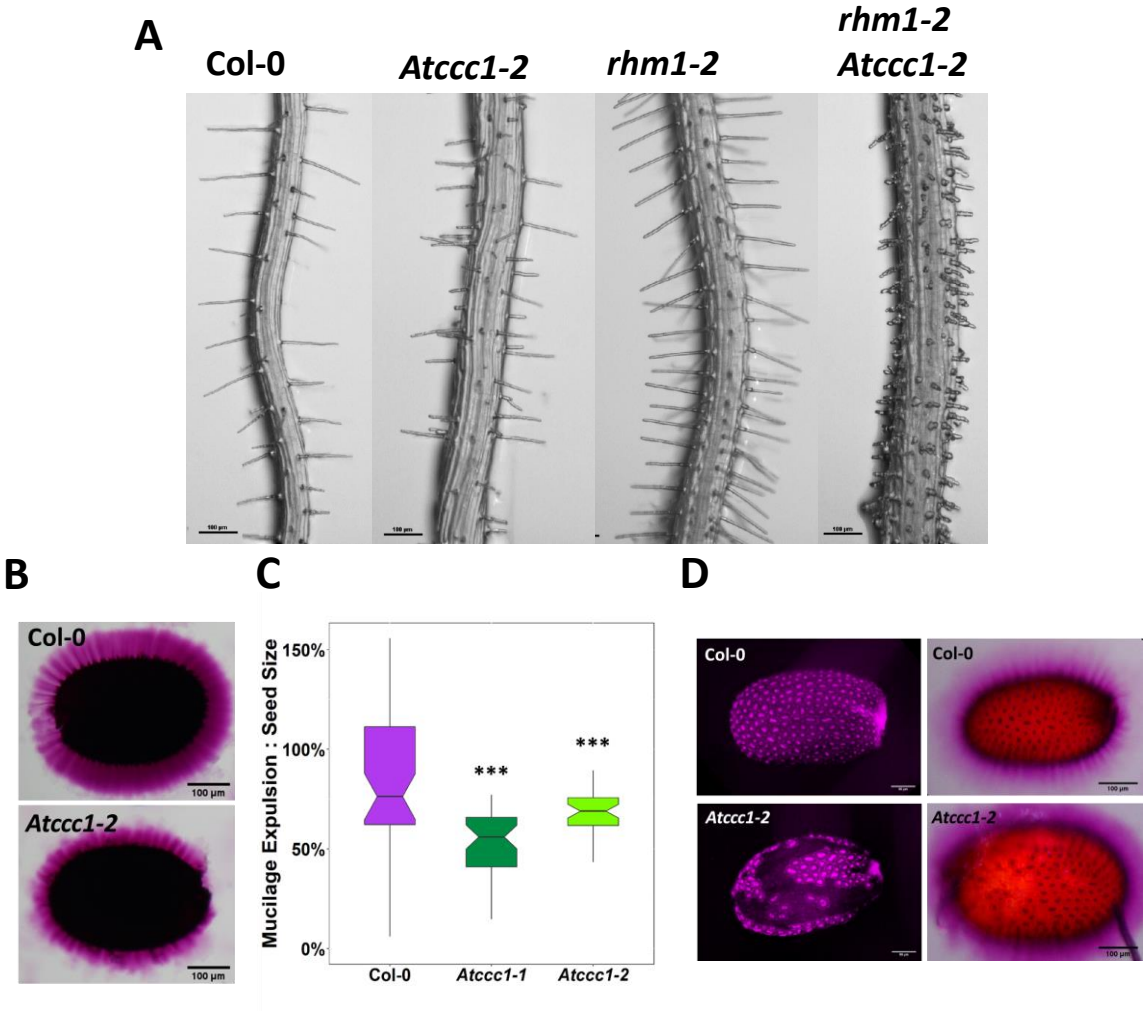

Figure 5: Loss of *Atccc1* impacts the cell wall. A) A double mutant of the *Rhamnose Synthase 1* (*rhm1-2*) and *Atccc1* showed an extremely severe root hair phenotype, beyond the additive effects of either single knockout. B-C) Imbibed *Atccc1* seeds have reduced mucilage, seed mucilage stained with ruthenium red. Scale bars = 100 µm, n = 41-43, student t-test D) Seed coat columella cells are irregularly developed in *Atccc1*, shown by autofluorescence (left panel) and stereo microscopy (right panel), scale bars = 100 µm.

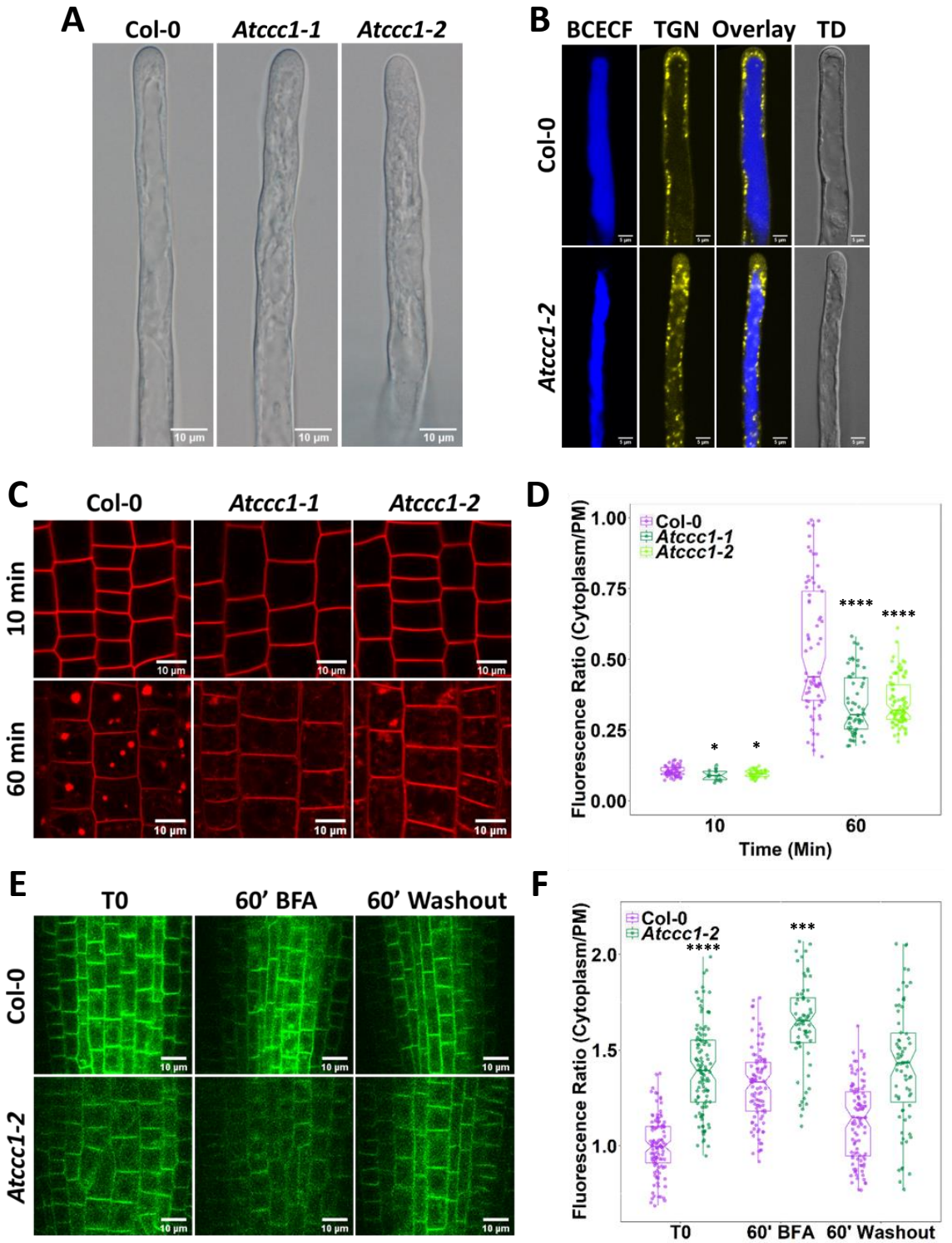

Figure 6: AtCCC1 is important for endomembrane trafficking. A) DIC imaging of root hairs shows strongly increased cytoplasm in *Atccc1* compared to Col-0 wildtype (see also suppl. videos 11-13). Scale bars = 10 µm. B) BCECF staining of the vacuole (blue) in plants expressing the TGN/EE marker VHAa1-mRFP (yellow) showing altered vacuolar morphology in *Atccc1*. Scale bars = 5 µm. C-D) Endocytosis rate is reduced in *Atccc1*, C) Col-0 and *Atccc1* root tip cells, stained with FM4-64 (red), and treated with BFA for 10 min or 60 min, D) fluorescent ratio of plasma membrane to cell internal fluorescence. Scale bars = 10 µm, n = 56-89, students t-test comparing *Atccc1* and wildtype. E-F) Localisation pattern of auxin transporter PIN1 is altered in *Atccc1*. E) Col-0 wildtype and *Atccc1* plants stably expressing PIN1-GFP (green), expression driven by *PIN1* promoter. *Atccc1* plants showing reduced plasma membrane localisation of PIN1-GFP and a reduced reaction to BFA treatment. Scale bars = 10 µm, n = 13-27, students t-test comparing *Atccc1* and wildtype.

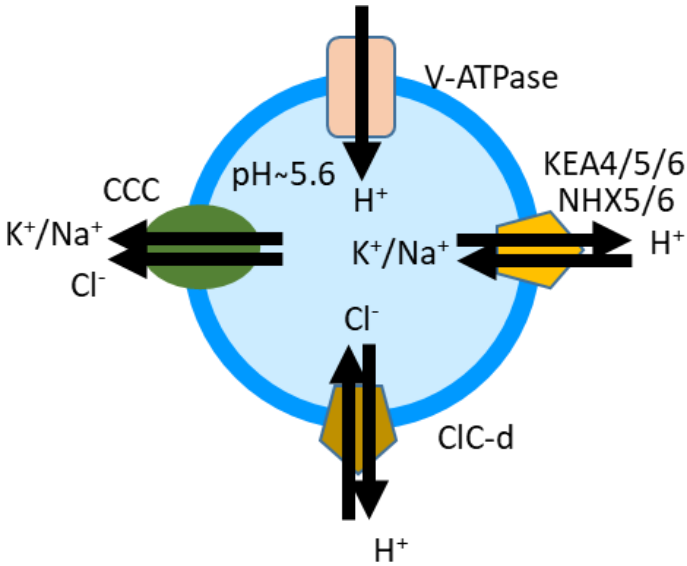

Figure 7: Proposed model of ion and pH regulation in the TGN/EE, with CCC as the missing component. The V-ATPase proton pump, the cation-proton exchangers NHX5, NHX6, KEA4, KEA5 and KEA6 and the anion proton exchanger CLC-d have been previously shown or proposed to be important for pH regulation in the TGN/EE lumen (Sze and Chanroj, 2018). CCC1s are candidates for providing an electroneutral ion shunt, completing the regulatory transport circuit.